




Small Language Model-based Control for BBR over Low Earth Orbit Satellite Internet

Rakshitha De Silva , Shiva Raj Pokhrel  *Senior Member, IEEE* and Jonathan Kua  *Member, IEEE*

Abstract—Low Earth Orbit (LEO) satellite Internet introduces rapid path variability, intermittent capacity shifts, and non-terrestrial delay dynamics that challenge transport-layer congestion control. Although Bottleneck Bandwidth and Round-trip propagation time (BBR) achieves high throughput in such environments, its aggressive bandwidth probing can cause excessive retransmissions and unstable pacing over LEO links. This paper presents a global experimental evaluation of BBR over a SpaceX Starlink testbed spanning six geographically distributed AWS endpoints and compares its behaviour against Cubic, Vegas, and Hybla under isolated and competing traffic scenarios. The measurements show that BBR consistently delivers superior throughput but incurs significantly higher retransmission overhead, revealing a critical throughput–stability trade-off in LEO satellite Internet. To address this limitation, we propose a Small Language Model (SLM)-guided BBR adaptation framework that learns phase-safe pacing-gain decisions from real Starlink traces. The framework combines a structured BBR state encoder, LoRA-based parameter-efficient fine-tuning, and a constrained networking head to generate feasible pacing actions with low inference latency. Evaluation using GPT-2, T5, GPT-Neo, and SmolLM2 shows that lightweight SLMs can retain BBR’s throughput advantage while substantially reducing retransmissions, with performance comparable to larger language models but at much lower computational cost.

Index Terms—Bottleneck Bandwidth and Round-trip propagation time (BBR), Network measurements, Starlink Internet, Small Language Model (SLM)

I. INTRODUCTION

Low Earth Orbit (LEO) satellite mega-constellations [1] have emerged as a cornerstone of next-generation global communications, enabling wide-area broadband with significantly lower latency than traditional satellite systems. SpaceX Starlink represents the largest and most mature constellation to date, alongside efforts such as Eutelsat OneWeb and Amazon Kuiper. Google’s Bottleneck Bandwidth and Round-trip propagation time (BBR) Congestion Control Algorithm (CCA) [2] marks a paradigm shift in Transmission Control Protocol (TCP) congestion control by explicitly modeling bottleneck bandwidth and propagation delay rather than relying on loss-based detection. Its latest iteration, BBRv3 [2]¹, refines probing and pacing to optimize throughput, latency, and fairness across diverse conditions. In parallel, Small

Language Models (SLMs), a subclass of Large Language Models (LLMs) designed to operate under strict compute, memory, and latency constraints [3], retain meaningful language understanding within tight hardware budgets, making them well suited to edge, mobile, and embedded settings [4] and, in particular, to network-driven tasks that demand real-time inference close to the data source [5].

The recent surge in mega constellations has prompted industry and academia to optimize data transmission over satellite networks, generalizing it as a replacement and extension of well-established terrestrial networks [6]. Internet congestion control is a well-explored problem in the literature, yet inherited dynamics and transmission delays make it especially challenging in satellite networks [7], [8]. Many works have produced comparative analyses of Congestion Control Algorithms (CCAs) over satellite networks [6], [9], highlighting these associated challenges. To this end, a significant number of contributions have been made in developing new CCAs for satellite Internet. The most notable works include, but are not limited to: LeoCC [10], TCP-Peach [7], REFWA [8], and StarQUIC [11].

Several studies have proposed refinements to BBR to address fairness limitations and adapt its behavior to specific networking scenarios. Modest BBR [12], BBR-CWS [13], and BBR-ACD [14] mitigate BBR’s aggressive probing by refining congestion window control and congestion detection, improving coexistence with loss-based flows and stability under shared bottlenecks. More recent works, such as BBR-R [15] and BBR-EFRA [16], focus on multi-flow competition and Round Trip Time (RTT) fairness, respectively, reducing bandwidth monopolization and unfairness across heterogeneous paths. In parallel, delay-control adaptations similar to BBR-ES [17] extension for low-latency applications.

Recent efforts along this line leveraged Deep Reinforcement Learning (DRL) to replace or augment rule-based CCAs, as demonstrated in iCoCoA [18], enabling adaptive rate control under dynamic network conditions. Several works have specifically targeted satellite networks, applying DRL to optimize congestion control in Low Earth Orbit (LEO) constellations [19], [20], Software Defined Network (SDN)-enabled satellite architectures [21], and deep-space communication scenarios [22], where high RTTs, intermittent links, and handovers challenge conventional CCAs. These approaches consistently show that learning-based controllers can better capture complex state–action relationships than handcrafted heuristics, leading to improved throughput, latency, and robustness. More recently, the paradigm has expanded beyond DRL toward Large Language Models (LLMs), with LLM-based

This work is supported by SmartSat CRC, whose activities are funded by the Australian Government’s CRC Program.

R. De Silva, S. R. Pokhrel and J. Kua are with the IoT & Software Engineering Research Lab, School of Information Technology, Deakin University, Geelong, VIC 3125, Australia (e-mail: rakshitha.desilva@deakin.edu.au; shiva.pokhrel@deakin.edu.au; jonathan.kua@deakin.edu.au).

¹For the rest of the paper, if not stated otherwise, Bottleneck Bandwidth and Round-trip propagation time (BBR)v3 is referred to as BBR.

queue management [23], cross-layer network tasks [24], and LLM-driven cognitive spectrum adaptation [25], illustrating the potential of LLMs as high-level decision engines for network-aware control in next-generation satellite systems. These advances, together with growing on-device and edge LLM deployments [5], [26], motivate us to leverage Small Language Models (SLMs) to address elevated retransmission in BBR over Starlink.

In this work, we have the following key contributions:

- We design and implement a global Starlink performance testbed across six cities: Ohio, S ã o Paulo, London, Mumbai, Tokyo, and Sydney, on the Amazon Web Services (AWS) platform, and present a comprehensive empirical evaluation of BBR under individual and competing uplink/downlink scenarios.
- We propose a SLM-based approach for smooth BBR pacing gains, comprising a state encoder that projects BBR numerical data into a language model-compatible feature space, a Low Rank Adaptation (LoRA)-based Reinforcement Learning (RL) pipeline that distills language models for accelerated prediction of pacing gains, and a task-specific language model head that eliminates invalid action generation.

We build a global, distributed testbed over the Starlink network, leveraging AWS infrastructure to study the empirical behavior of BBR. The testbed expands to six AWS endpoints centered on Melbourne, Australia, and we compare BBR performance with three leading CCAs: Cubic [27], Vegas [28], and Hybla [29]. The observations highlight a throughput advantage, as BBR significantly outperforms all three baseline CCAs in both uplink and downlink, under isolated and competitive scenarios, fully utilizing the available Starlink Ku-band. The larger congestion window achieved through the probing mechanism is the primary facilitator of this advantage. Moreover, this throughput advantage is realized within comparatively similar RTT and RTT-variance margins to other CCAs. Compared to benchmark CCAs, the primary downside we observed is the notably high number of TCP retransmissions, in all four test scenarios, across all six locations. This is a drawback resulting from the intentional aggressive probing for high bandwidth in the Starlink network, which often leads to inaccurate bottleneck estimates in dynamic network paths. Exploiting the collected data from the distributed testbed, we proposed a SLM driven BBR approach, reducing the inherent aggressiveness through smooth pacing gains. Due to the lightweight deployment advantages and inherited generalization capabilities of SLMs, our developed model represents a further step towards intelligence-driven network control for satellite Internet.

Moreover, we formulate the BBR CCA problem as offline return-conditioned policy learning over measurement traces. For tractability, we evaluate the proposed approach with four celebrated SLMs, viz., GPT-2¹, T5², GPT-Neo³, SmolLM2⁴, and an LLM (LLaMA 3.2⁵ >3B parameters). For reproducibility, we provide the complete implementation, including preprocessing, SLM fine-tuning, reward construction, pacing-gain inference and evaluation scripts at: <https://github.com/>

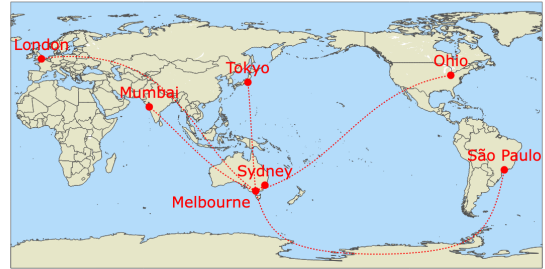


Fig. 1: Global testbed setup centered on Melbourne, expanding to AWS endpoints in six cities: Ohio, S ã o Paulo, London, Mumbai, Tokyo, and Sydney.

MPTCP-FreeBSD/lm-bbr-starlink.git.

II. OUR EXPERIMENT: OBSERVATIONS AND FINDINGS

A. Testbed Setup

As illustrated in Fig. 1, we set up six servers in main cities distributed globally, namely Ohio, S ã o Paulo, London, Mumbai, Tokyo, and Sydney. We leveraged AWS Linux cloud instances for this distributed server setup, and the local portion of the setup was based on the university premises in Melbourne, Australia. The user terminal consists of a Starlink latest-generation standard kit with a UTA-232 model dish. A Linux-based local server was connected to the Starlink terminal through a Category 5e Ethernet connection, creating a perpetual test environment. Furthermore, we assume the AWS cloud instances to provide a consistent network connection throughout the geographically distributed cloud instances. To test TCP CCA performance over the testbed, we leverage *iperf3*, an open-source network testing tool used to measure the maximum achievable bandwidth and performance over network connections. It provides detailed metrics on CCA performance such as throughput, retransmissions, congestion window, receiver advertised window, RTT, and RTT-variance, making it widely used for network diagnostics and benchmarking.

We implemented an automated measurement framework using *iperf3*, in which each remote server and local end was sequentially configured for specified CCA. We then performed forward and reverse tests for uplink and downlink for individual CCA data collections. To evaluate the CCA behavior as parallel and competing streams, we implemented isolated namespaces for each CCA in each Linux network instance and followed a similar data collection process. Special care was taken to synchronize server startup, ensuring data flushing before retrieval, and preserve isolation across CCAs to avoid inter-flow interference, thereby enabling fair and repeatable CCA benchmarking under identical network conditions. Data was collected for a 300-second capture window for each CCAs in all four test scenarios, and the experiment was carried out during the first week of August 2025.

¹<https://huggingface.co/openai-community/gpt2>

²https://huggingface.co/docs/transformers/en/model_doc/t5

³<https://www.eleuther.ai/artifacts/gpt-neo>

⁴<https://ollama.com/library/smolm2>

⁵<https://www.llama.com/>

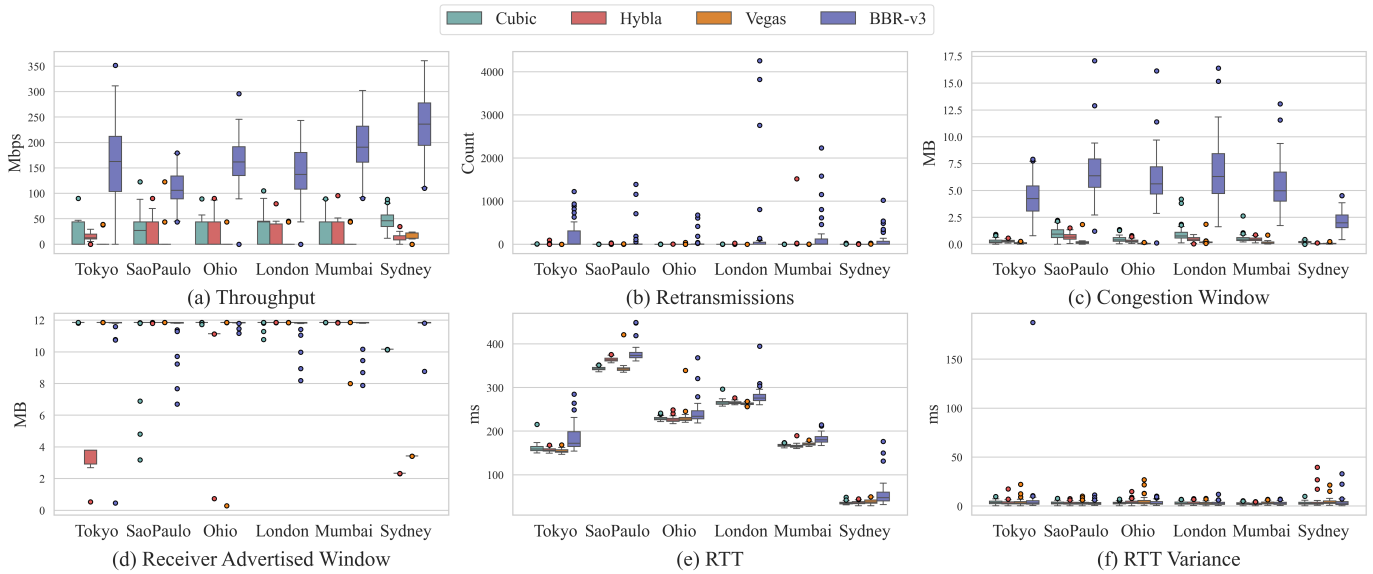


Fig. 2: Downlink data for independent CCA streams across the Starlink testbed.

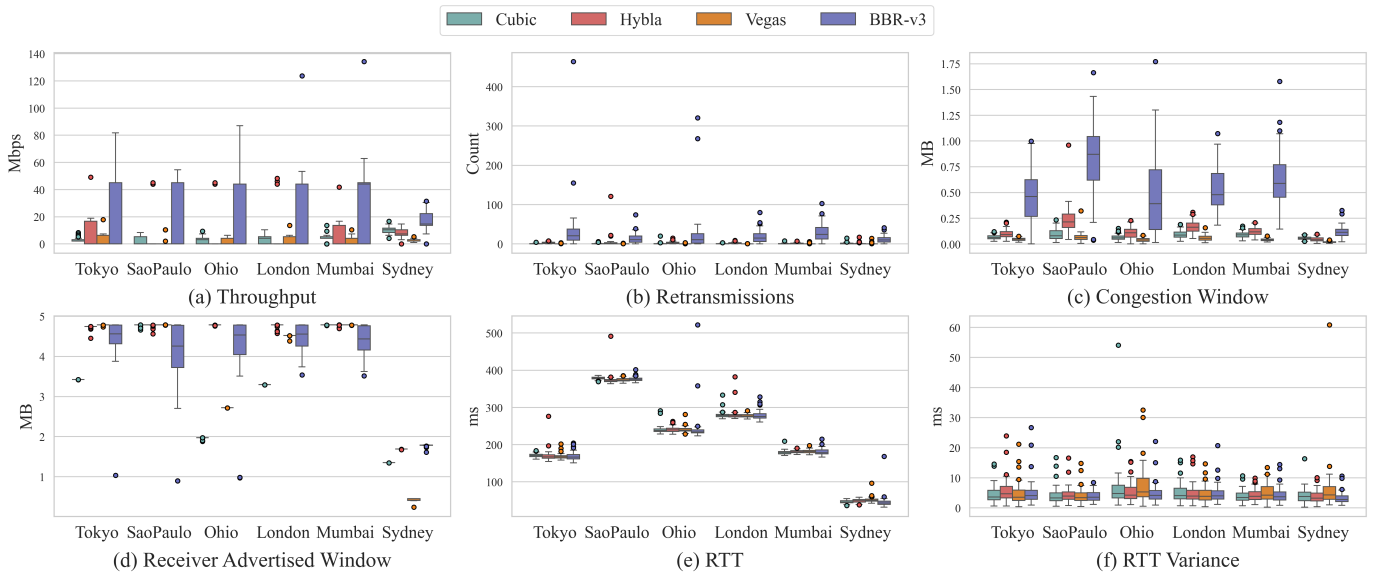


Fig. 3: Uplink data for independent CCA streams across the Starlink testbed.

B. Evaluation: BBR over Starlink

1) *On Independent Noncompetitive Streams*: Across both independent download and upload streams, BBR consistently achieved the highest throughput of all evaluated CCAs at every test location. Downlink median (Q_2) values exceed 100 Mbps in São Paulo, and upper whiskers approach 350 Mbps in Sydney (Fig. 2(a)), while uplink throughput, though lower overall, still reaches upper whiskers exceeding 80 Mbps (Fig. 3(a)). This performance came with markedly higher retransmissions than Cubic, Vegas, and Hybla, which all remained near-negligible. In downlink, BBR’s retransmissions peaked in Tokyo ($Q_3 > 300$) and Mumbai ($Q_3 > 100$), while in uplink they reached $Q_2 \in [20, 30]$ with maxima near 70, concentrated in high-RTT locations (Fig. 2(b), Fig. 3(b)). BBR’s congestion window was substantially larger than the other CCAs in both directions (min $Q_2 > 0.4$ MB in Sydney for uplink) with the highest overall variance, enabling higher Bandwidth-Delay

Product (BDP) utilization (Fig. 2(c), Fig. 3(c)). RTTs were location-driven rather than CCA-driven, highest in São Paulo ($Q_2 \approx 350$ ms) and lowest in Sydney ($Q_2 \approx 50$ ms), with RTT variance remaining modest and similar across all CCAs (Fig. 2(e),(f), Fig. 3(e),(f)).

Despite its significantly higher throughput and retransmissions, BBR maintained RTT and RTT variance comparable to the benchmark CCAs. The steady, similar RTT variance indicates that its retransmission overhead stemmed primarily from BBR’s own aggressive probing rather than from Starlink’s dynamics. This reflects a clear trade-off, BBR operates closer to link capacity at the cost of stability, whereas the traditional loss and delay-based CCAs (Cubic, Vegas, Hybla) underutilize available capacity, confirming their limited effectiveness over Starlink. By relying on a model-based approach, BBR bypasses the RTT-dependence of conventional CCAs, making it an efficient choice for Starlink’s dynamic

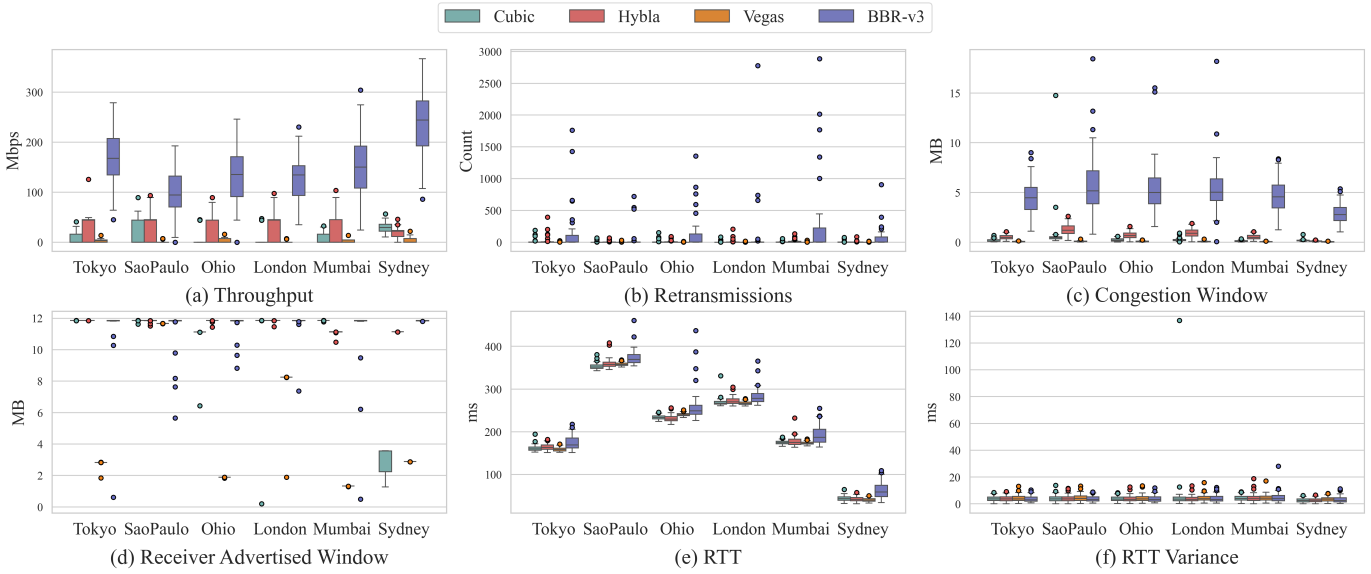


Fig. 4: Downlink data for parallel CCA streams over the global distributed Starlink testbed.

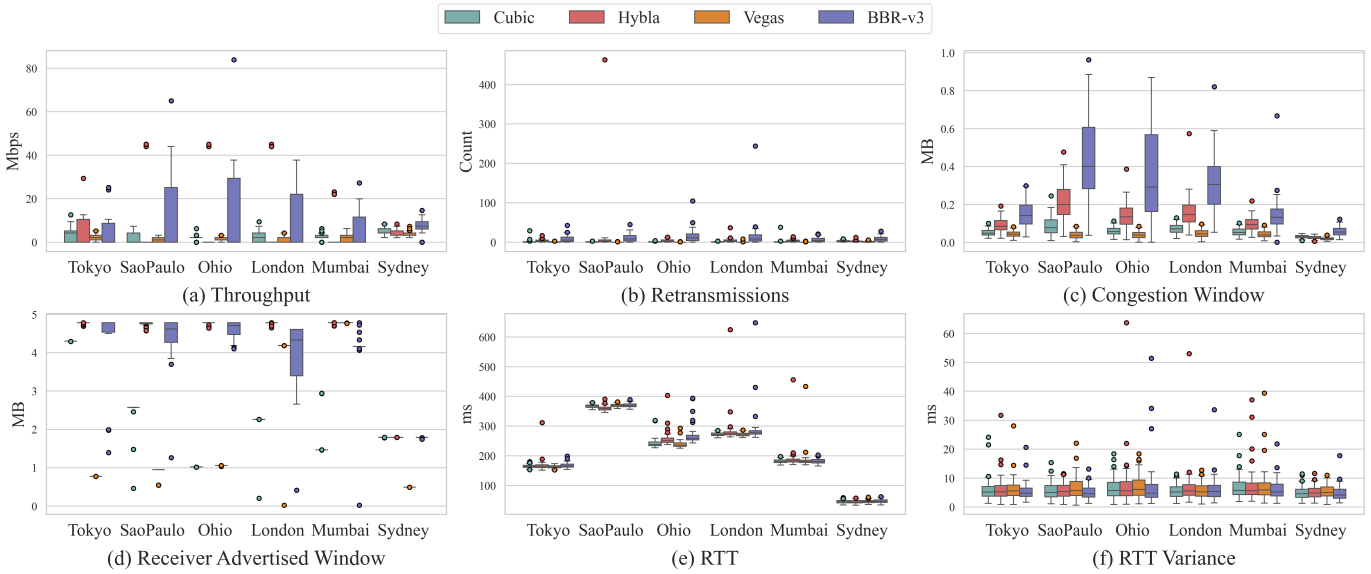


Fig. 5: Uplink data for parallel CCA streams over the global distributed Starlink testbed.

LEO environment. Overall, BBR demonstrates the strongest suitability for high-throughput operation over Starlink, though retransmission mitigation strategies are needed to improve its robustness.

2) *On Parallel Competitive Streams:* Under parallel, competitive stream conditions, BBR consistently achieved the highest median throughput across all test sites in both directions, with downlink medians exceeding 130 Mbps in London and 240 Mbps in Sydney, with peaks above 350 Mbps (Fig. 4(a)). In the uplink direction, upper whiskers exceeded 35 Mbps, with Sydney achieving the best aggregated performance (Fig. 5(a)). By contrast, the benchmark CCAs struggled to sustain capacity under contention. Vegas frequently dropped to near-zero median downlink throughput, while Hybla outperformed Cubic and Vegas in selected locations ($Q_2 \approx 44$ Mbps downlink) yet degraded sharply in high-RTT sites such as São Paulo, London, and Ohio. This dominance came at the cost of the highest retransmissions in every location, with downlink

upper whiskers exceeding 400 packets in Mumbai and 200 in Tokyo and Ohio, and uplink medians above 6 packets reaching maxima beyond 30 in high-RTT locations (Fig. 4(b), Fig. 5(b)). BBR also sustained the largest congestion windows (often $Q_2 > 5$ MB in downlink), enabling high in-flight data volumes while the other CCAs remained window-limited (Fig. 4(c), Fig. 5(c)). RTT distributions showed only marginally higher variability for BBR in downlink, with RTT variance profiles following a similar pattern across all four CCAs and recording the highest RTT in São Paulo and the lowest in Sydney (Fig. 4(e),(f), Fig. 5(e),(f)).

BBR consistently dominated competitive downlink and uplink capacity under parallel-stream conditions on Starlink, and similar to independent streams, its aggressive bandwidth probing delivered superior throughput at the cost of significantly increased retransmissions. The loss-based (Cubic) and delay-based (Vegas) CCAs instead sacrificed bandwidth efficiency to preserve stability and lower queuing pressure. Hybla only

Algorithm 1 Creating Experience Pool from Starlink BBR Datasets

```

1: Concatenate iperf3 BBR captures into a data-frame
   with  $\{t, b_t, \tau_t, cwnd_t, rwnd_t, RTT_t, RTTvar_t\}$  values
2: for all dataset specifications  $d \in \mathcal{D}_{BBR}$  do
3:   Insert identifiers: Location flag  $-L_j$ , Stream flag  $-S_k$ ,
4:   Phase Detection:
5:   Compute smoothed rolling mean throughput  $\bar{b}(t)$ .
6:   Compute deviation: Eq. (1)
7:   Set thresholds  $d_\uparrow \leftarrow \kappa\sigma_d$ ,  $d_\downarrow \leftarrow -\kappa\sigma_d$ 
8:   Set initialize pace state ProbeBW_CRUISE for all
   samples
9:   Scan for local maxima above  $d_\uparrow$  to mark
   ProbeBW_UP
10:  For each ProbeBW_UP event, scan forward for local
   minima below  $d_\downarrow$  to mark ProbeBW_DOWN
11:  Mark subsequent 6 samples after ProbeBW_DOWN as
   ProbeBW_CRUISE
12:  Phase-Constrained Gain Selection:
13:  Compute per location/stream capacity estimate
    $B_{\max} \leftarrow \max_t bps(t)$ 
14:  Compute utilization proxy  $\bar{B}_i \leftarrow b_i / \max_j b_j$ 
15:  for all candidate gains  $g \in \mathcal{A}_{\phi_i}$  do
16:    Estimate  $\hat{B}_i(g)$  and  $\hat{\tau}_i(g)$  trace-driven model
17:    Compute  $R(s_i, g)$ 
18:  end for
19:  Select  $a_i^* \leftarrow \arg \max_{g \in \mathcal{A}_{\phi_i}} R(s_i, g)$ 
20:  Append  $(s_i, a_i^*, R(s_i, a_i^*))$  to  $\mathcal{D}_{BBR}$ 
21: end for
22: return  $\mathcal{D}_{BBR} =$ 
    $\{state \in \{L_j, S_k, t_i, b_i, \tau_i, cwnd_i, rwnd_i, RTT_i, RTTvar_i\},$ 
    $\mathcal{A} \in \{S_{UP}, S_{DOWN}, S_{CRUISE}\}, reward\}$ 

```

partially mitigated RTT-induced penalties and remained highly sensitive to contention, exhibiting unstable, burst-driven behavior. Notably, despite its marginally higher RTT distribution in download streams, BBR maintained RTT and RTT variance comparable to the benchmark CCAs. Overall, BBR is best suited for capacity-dominant transfers over Starlink, whereas the more conservative CCAs favor predictable delay at the expense of throughput.

III. PROPOSED FINETUNING SLM FOR BBR OVER STARLINK

This section describes the data-processing pipeline developed to convert raw iperf3 BBR logs into structured data and SLM finetuning approach, as illustrated in Fig. 6. The discussion is developed inline with SLMs, however, it is important to note that the proposed approach is compatible with LLMs, as emphasized in the result evaluation section later in this work.

A. Reinforcement Learning Pipeline

As discussed in § II, iperf3 BBR logs contain per second measurements of throughput (b), congestion window ($cwnd$), RTT (RTT), retransmissions (τ),

receiver advertised window ($rwnd$), RTT (RTT) and RTT-variance (RTTvar). Thus, we consider a tuple of $\{t_i, b_i, \tau_i, cwnd_i, rwnd_i, RTT_i, RTTvar_i\}$ for each interval i , where t_i is the respective time index. In BBR bandwidth probing phases, pacing gain changes in three steps, in ProbeBW_DOWN, it goes down to 0.9, in ProbeBW_CRUISE and ProbeBW_REFILL, it stabilizes at 1, and in ProbeBW_UP, it goes up to 1.25 [2]. This fixed pacing gain strategy may cause the CCA’s adjustment to lag when the bandwidth deviates, particularly in highly variable environments like LEO satellite networks [30], [31].

1) *Discrete Pacing Gain Selection*:: Instead of the three-step pacing gain scheme, we introduce a granular discrete approach to counter the inherent aggressiveness. Let \bar{b}_i denote a centered rolling-mean smoothed throughput estimate, and we define d_i as:

$$d_i = b_i - \bar{b}_i, \quad (1)$$

with standard deviation $\sigma_d = \text{std}(d_i)$. An index sample is classified as ProbeBW_UP if $d_i > 0.7\sigma_d$ and d_i forms a local maximum, and as ProbeBW_DOWN if $d_i < -0.7\sigma_d$ and is a local minimum. A fixed pacing gain region of six sample cycles is inserted immediately following a ProbeBW_DOWN event detection, aligning with the BBR state machine.

To model BBR pacing behavior at a finer resolution, we discretize the gain around cruise pacing gain as $\mathcal{S}_{UP} = \{1.05, 1.10, 1.15, 1.20, 1.25\}$, $\mathcal{S}_{DOWN} = \{0.90, 0.92, 0.94, 0.96, 0.98\}$ and $\mathcal{S}_{CRUISE} = 1.00$. We leveraged a continuous gain estimate model derived as [31]:

$$G_i^\uparrow = \frac{3}{\bar{B}_i + 2}, \quad G_i^\downarrow = \frac{\bar{B}_i + 1}{2}, \quad (2)$$

where $\bar{B}_i = b_i / \max_j b_j$ is a normalized rate-based throughput utilization estimate. Thus, we select gain as the nearest discrete value permitted by the detected macro-phase:

$$G_i = \begin{cases} \arg \min_{g \in \mathcal{S}_{UP}} |g - G_i^\uparrow|, & \text{phase}_i = \text{UP}, \\ \arg \min_{g \in \mathcal{S}_{DOWN}} |g - G_i^\downarrow|, & \text{phase}_i = \text{DOWN}, \\ 1.00, & \text{phase}_i = \text{CRUISE}. \end{cases} \quad (3)$$

2) *Hybrid Utilization and Reward Construction*:: We define normalized throughput and retransmission reward components as:

$$B_i = \min\left(\frac{b_i}{B_i^{\text{ref}}}, 1\right), \quad (4)$$

$$\bar{\tau}_i = \tanh\left(\frac{\tau_i}{\bar{\tau}_i^{\text{ref}}}\right). \quad (5)$$

where B_i^{ref} and $\bar{\tau}_i^{\text{ref}}$ are interpreted as moving 95th percentile references for throughput and retransmissions where:

$$B_i^{\text{ref}} = Q_{0.95}(b_{i-w:i+w}), \quad (6)$$

$$\bar{\tau}_i^{\text{ref}} = Q_{0.95}(\tau_{i-w:i+w}) + 1, \quad (7)$$

and $Q_p(\cdot)$ denotes the empirical percentile and w is the window size. A saturating function is leveraged in encapsulating retransmission to eliminate the effect of a large spike in the captured BBR data.

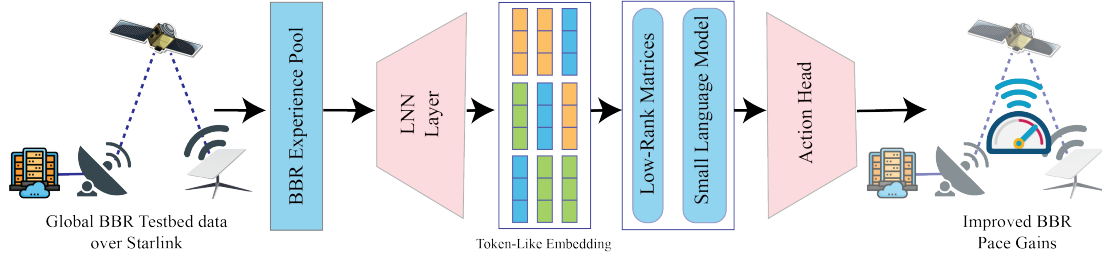


Fig. 6: An overview of the language model finetuning process for improved BBR.

TABLE I: Hyperparameter settings used in reward and loss construction.

Parameter	Value	Description
w	10	Half-window for rolling percentile estimates
κ	0.7	ProbeBW phase-detection threshold scale
λ_1	0.5	Retransmission penalty weight
λ_2	0.1	Aggressive probe-up penalty weight
α	1.5	Superlinear probe-loss growth factor
β	5	Softplus probe-activation sharpness
ϵ	10^{-3}	Minimum non-zero loss floor
κ_{down}	0.5	Probe-down retransmission reduction factor

Throughput may saturate with excessive queue buildups, and delay alone may remain low during short probing phases even when bandwidth is underutilized. Therefore, to represent congestion effects in the reward function, a hybrid utilization estimate embodying rate and delay is incorporated. Let $\text{RTT}_{\min} = \min_j \text{RTT}_j$ considering a rolling window, and define the queuing delay $qd_i = \max(\text{RTT}_i - \text{RTT}_{\min}, 0)$. A bounded queue reference can be computed as:

$$q_i^{\text{ref}} = \min(Q_{0.95}(qd_{i-w:i+w}), 0.15 \text{RTT}_{\min}). \quad (8)$$

Thus, the rate-based and delay-based utilizations are defined as:

$$U_i^{\text{rate}} = B_i, \quad (9)$$

$$U_i^{\text{delay}} = \min\left(\frac{qd_i}{q_i^{\text{ref}}}, 1\right), \quad (10)$$

Thus, the hybrid utilization factor can be given as:

$$U_i = \max(U_i^{\text{rate}}, U_i^{\text{delay}}). \quad (11)$$

A penalty is introduced to penalize aggressive pacing when $G_i > 1.0$:

$$l_i = \max(G_i - 1, 0). \quad (12)$$

Thus, the reward function is defined as:

$$r_i = B_i - \lambda_1 C_i - \lambda_2 U_i l_i, \quad (13)$$

where $\lambda_1 = 0.5$ and $\lambda_2 = 0.1$. Thus, we define an experience pool dataset along the RL framework as $\mathcal{D}_{\text{BBR}} = \{\text{state}, \text{action}, \text{reward}\}$, incorporating the states: $s_i \in \{L_{i,j}, S_{i,k}, t_i, b_i, \tau_i, \text{cwnd}_i, \text{rwnd}_i, \text{RTT}_i, \text{RTTvar}_i\}$ where $L_{i,j}$ is a location flag and $S_{i,k}$ is a stream identification flag for the respective dataset of the four types collected with the distributed testbed. The action set is defined as: $a_i \in \{\mathcal{S}_{\text{UP}}, \mathcal{S}_{\text{DOWN}}, \mathcal{S}_{\text{CRUISE}}\}$. The framework used in this process is further detailed in Algorithm 1 and hyperparameters are defined in Table I.

We select the pacing gain from the finite action space $\mathcal{A} = \{0.90, 0.92, 0.94, 0.96, 0.98, 1.00, 1.05, 1.10, 1.15, 1.20, 1.25\}$. (14)

To preserve BBR phase consistency, the feasible set is

$$\mathcal{A}_{\phi_i} = \begin{cases} \{1.05, 1.10, 1.15, 1.20, 1.25\}, & \phi_i = \text{BW_UP}, \\ \{0.90, 0.92, 0.94, 0.96, 0.98\}, & \phi_i = \text{BW_DOWN}, \\ \{1.00\}, & \phi_i = \text{BW_CRUISE}. \end{cases} \quad (15)$$

For each candidate $g \in \mathcal{A}_{\phi_i}$, the trace-driven models estimate the delivered throughput $\hat{B}_i(g)$ and retransmission cost $\hat{\tau}_i(g)$. The reward is

$$R(s_i, g) = \frac{\hat{B}_i(g)}{B_i^{\text{ref}}} - \lambda_1 \frac{\hat{\tau}_i(g)}{\tau_i^{\text{ref}}} - \lambda_2 U_i \max(g - 1, 0), \quad (16)$$

where U_i denotes hybrid utilization. The expert label is the feasible gain that maximizes this reward:

$$a_i^* = \arg \max_{g \in \mathcal{A}_{\phi_i}} R(s_i, g). \quad (17)$$

Thus, the experience pool is

$$\mathcal{D}_{\text{BBR}} = \{(s_i, a_i^*, R(s_i, a_i^*))\}_{i=1}^N, \quad (18)$$

providing phase-safe expert labels for offline return-conditioned policy learning.

B. State Encoder

To transform `iperf3` generated BBR state information into representations compatible with SLM architectures, we employ a structured feature encoding mechanism tailored to the heterogeneous requirements of the selected models. A series of fully connected layers is first used to process the scalar inputs produced by our Starlink-BBR global testbed. SLMs impose varying context window constraints; for example, GPT-2 supports sequences up to 1024 tokens, and T5 operates with a 512-token span. Thus, dimensional alignment between the encoded features and the target model's token space is essential. Therefore, we incorporate a Linear Neural Network (LNN) layer that systematically maps the extracted features into embedding dimensions compatible with each model's context window. This design ensures architectural coherence and facilitates seamless integration with SLM backbones of different scales and configurations, converting the extracted features into a matching context window. Layer normalization is subsequently applied to the projected embeddings to enhance numerical stability, mitigating Covariate shift and promoting efficient optimization. Therefore, the state encoder

Algorithm 2 SLM-based BBR for Starlink Internet

Require: Transformed structured \mathcal{D}_{BBR} to trainable data, action sequence \mathcal{A} and feature dimensions n_f , where $\mathbf{x}_t = [R_t, s_t^{(1)}, \dots, s_t^{(n_s)}, a_t]^T \in \mathbb{R}^{n_r}$

Part I - State Encoder:

- 1: Initialize State tensor $\mathbf{S} \in \mathbb{R}^{B \times T \times n_f \times 1}$ with embedding dimension d' , batch size B and sequence length T
- 2: Initialize FC layers $\{\text{FC}_i(\cdot)\}_{i=1}^{n_f}$ with LeakyReLU activation
- 3: Reshape state tensor: $\mathbf{S} \leftarrow \text{reshape}(\mathbf{S}, (B \cdot T, n_f, 1))$
- 4: **for** $i = 1$ to n_f **do**
- 5: Extract scalar feature: $s_i \leftarrow \mathbf{S}(i)$
- 6: Encode feature using FC layer: $\mathbf{f}_i \leftarrow \text{FC}_i(s_i)$
- 7: Reshape encoded feature: $\mathbf{F}_i \leftarrow \text{reshape}(\mathbf{f}_i, (B, T, d))$
- 8: **end for**
- 9: **return** $\{\mathbf{f}_1, \mathbf{f}_2, \dots, \mathbf{f}_{n_f}\}$

Part II - Low-Rank Adaptation:

- 10: Initialize matrices A and B with random weights θ_{lr}
- 11: **for** epoch = 1 : epochs **do**
- 12: **for** data batch = 1 to data batches in \mathcal{D}_{BBR} **do**
- 13: Get the forward pass model output
- 14: Compute the loss Eq. (20)
- 15: Update θ_{lr}
- 16: **end for**
- 17: **end for**
- 18: **return** $W_\tau \leftarrow W_\theta + A_\tau B_\tau$

Part III - Offline RL Policy with Language Model Head:

- 19: Embed actions (\mathbf{E}_a), returns (\mathbf{E}_r), and time steps (\mathbf{E}_t) as trainable linear mapping
- 20: Add temporal embeddings: $\mathbf{E}_a \leftarrow \mathbf{E}_a + \mathbf{E}_t$, $\mathbf{E}_r \leftarrow \mathbf{E}_r + \mathbf{E}_t$
- 21: Encode state sequence using **State Encoder**
- 22: **for** $i = 1$ to n_f **do**
- 23: $\mathbf{E}_{s_i} \leftarrow \text{Embed}_{s_i}(\mathbf{F}_i) + \mathbf{E}_t$
- 24: **end for**
- 25: Construct autoregressive token sequence in \mathbf{x}_t^T format
- 26: Stack tokens over time to form input sequence \mathbf{X}
- 27: Truncate \mathbf{X} to model context length and apply layer normalization
- 28: Create attention mask \mathbf{M}
- 29: Compute hidden states using PLM:
 $\mathbf{H} \leftarrow \text{PLM}(\mathbf{X}, \mathbf{M})$
- 30: **if** residual connection enabled **then**
- 31: $\mathbf{H} \leftarrow \mathbf{H} + \mathbf{X}$
- 32: **end if**
- 33: Extract logits corresponding to action positions
- 34: Predict action logits: $\hat{\mathbf{A}} \leftarrow \text{ActionHead}(\mathbf{H})$
- 35: **return** $\hat{\mathbf{A}}$

approach prepares BBR data over Starlink in a form optimally structured for transformer-based processing while maintaining computational efficiency and robustness across diverse language model architectures.

C. LoRA Adaptation

To improve training efficiency, we adopt a LoRA strategy within the Parameter-Efficient Fine-Tuning (PEFT) framework [32]. This approach enables the reduction of parameters updated during training by freezing the majority of the pre-trained model weights of a language model. Let θ_{tot} denote the full parameter set of the SLM, which can be decomposed into frozen parameters θ_F and trainable parameters θ_T , such that $\theta_{\text{tot}} = \theta_F + \theta_T$. The corresponding weight matrices for the respective parameters can be denoted as W_{tot} , W_F , and W_T . Under the LoRA approach, the trainable weight update $W_T \in \mathbb{R}^{p \times q}$ is approximated using a low-rank decomposition. Specifically, we assume a rank r satisfying $r \ll \min\{p, q\}$ and express W_T as the product of two matrices, $A \in \mathbb{R}^{p \times r}$ and $B \in \mathbb{R}^{r \times q}$, such that $W_T = AB$. During fine-tuning, only the parameters in A and B are updated, while a significantly large portion of the original model weights remain fixed. This notably reduces computational and memory overhead while preserving the representational capacity of the pretrained SLMs for more generalized decision-making.

D. Language Model Head and Training

State encoder representations are subsequently forwarded to a dedicated *networking head*, which directly generates task-specific outputs. However, LLM hallucination, a well-known and explored issue within the field [33], can cause the generation of actions that fall outside the valid range. As a solution to this, the networking head is implemented as a trainable linear projection layer that maps the internal feature representations of the SLM. This matches the output to be within the desired space, in this work, modified BBR pacing gains. Moreover, since the model produces a single valid output within one inference step, the overall decision latency is significantly reduced.

Recall the RL-based pipeline leading to the experience pool, where $D_{BBR} = \{r_t, \mathbf{s}_t, \mathbf{a}_t\}_{t=1}^L \in \mathcal{D}_{BBR}$ and D_{BBR} denote a trajectory at L , the episode length. For each D_{BBR} we replace $r_t \leftarrow R_t = \sum_{i=t}^L r_i$, considering the cumulative rewards at s_t . Furthermore, state components, and action-related information are discretized as $s_t = \{s_t^1, \dots, s_t^g\}$ and $a_t = \{a_t^1, \dots, a_t^h\}$ exposing the incorporated information. The SLM is fine-tuned to learn return distributions using this data representation, with randomly sampled data sequences as:

$$\bar{D}_{BBR} = \{R_i, s_t^1, \dots, s_t^g, a_t^1, \dots, a_t^h\}_{i=t-w+1}^t \in \mathcal{D}_{BBR} \quad (19)$$

The optimization objective for training SLM action generation is defined in Eq. (20), where $L_H(\cdot)$ denotes the cross-entropy loss computed between the ground truth action $a_{t'}^j$ and the predicted action $\hat{a}_{t'}^j$. The loss is averaged across a prediction horizon of length w and across all m action dimensions.

$$L = \frac{1}{w} \sum_{t'=1}^w \sum_{j=1}^m L_H(a_{t'}^j, \hat{a}_{t'}^j) \quad (20)$$

The objective of this training strategy is to enable the SLM to internalize the relationship between system states and their associated return distributions. After training, the

TABLE II: Comparison of GPT-2, T5, GPT-Neo, and SmoLLM2 SLMs

Property	GPT-2	T5	GPTNeo	SmoLLM2
Parameters	137 M	237 M	132 M	388 M
Vocabulary Size	50,257	32,128	50,304	49,152
Hidden Size	768	768	768	960
Layers	12 d.	12 e. +	12 d.	32 d.
Attention Heads	12	12	12	15
FFN Size	3072	3072	3072	2560
Max Seq. Len	1024	512	2048	8192
Activation	GELU	ReLU	GELU	SiLU
Positional Encoding	Learned	Buckets	RoPE (25%)	RoPE

model is capable of synthesizing action sequences that are consistent with a desired performance objective. The overall process adapting SLMs to improve BBR pacing gains is further detailed in Algorithm 2.

IV. RESULT EVALUATION

A. Training and Validation

We separate the collected data detailed in § II as training and testing, grouping Ohio, São Paulo, London, Mumbai, and Sydney for training. Leveraging this real-world BBR data set, we evaluate the performance of our proposed approach using four SLMs: GPT-2, T5, GPT-Neo, and SmoLLM2. The primary selection criterion for these SLMs was the number of parameters; accordingly, we selected models with fewer than 400 M trainable parameters for this study. A summary comparison of the SLMs of interest is given in Table II. For the training and evaluation process, we used a workstation equipped with an Intel Xeon Gold 6346 CPU and two NVIDIA RTX 6000 GPUs, each with 96 GB of VRAM. To ensure a stable and efficient training process, we adopt mini-batches of 20 samples combined with gradient accumulation. Gradient clipping is also applied to constrain magnitude growth during backpropagation, thus preventing gradient explosion.

SLMs’ training performance was evaluated using cross-entropy loss for 150 epochs, as depicted in Fig. 7(a). T5 was the slowest to reduce the mean loss, requiring more than 50 epochs to reach stability. It was succeeded by GPT-Neo and GPT-2, and all three models exhibited similar loss patterns after convergence. However, SmoLLM2 deviated from the established pattern, reducing its mean loss relatively quickly and exhibiting fluctuations even after 100 epochs. Fig. 7(b) shows the mean training accuracy of the SLMs. After 30 epochs, all four SLMs converged in terms of mean accuracy even though SmoLLM2 displayed slight alterations, reflecting the loss pattern. Interestingly, GPT-2 and SmoLLM2 recorded similar accuracy patterns in the beginning, increasing rapidly, followed by T5. Comparatively, GPT-Neo was the slowest model to converge in respect of mean accuracy.

The primary outcome of the proposed LoRA approach is the reduction of training parameters in finetuning the SLMs to achieve improved BBR performance. Fig. 8(a) demonstrates a comparison of training parameters in SLMs of interest and

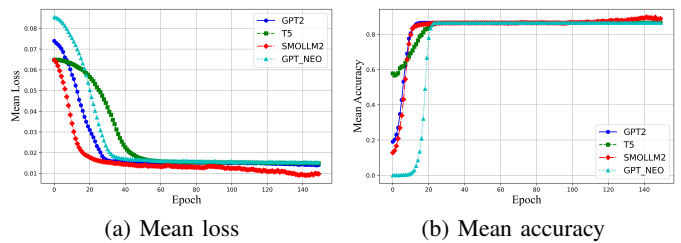


Fig. 7: Comparison of SLM training: (a) mean loss and (b) mean accuracy.

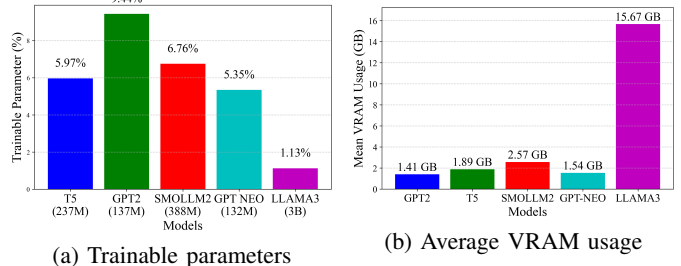


Fig. 8: Comparison of (a) trainable parameter percentages and (b) average VRAM usage in training.

LLaMA 3.2, a LLM with more than 3 B parameters, which we have used to benchmark the performance of the fine-tuned SLMs for the rest of this work. Respectively, only 9.44% GPT-2’s 137 M parameters, 5.97% of 237 M parameters in T5, 5.35% out of 132 M parameters in GPT-Neo, and 6.76% of SmoLLM2’s 388 M parameters are leveraged in training with the LoRA method. Comparatively, 1.13% out of 3 B parameters in LLaMA 3.2 is fine-tuned with the proposed method, thus reflecting on the significant reduction of the adapted trainable parameters. In addition, Video Random Access Memory (VRAM) utilization in training is significantly reduced through the LoRA approach as depicted in Fig. 8(b). As expected, SLMs’ VRAM usage is significantly lower compared to the LLaMA 3.2 model, which recorded 15.67 GB of mean VRAM consumption. Moreover, all four SLMs recorded a VRAM usage below 2.57 GB, SmoLLM2 registering the highest and GPT-2 with the lowest of 1.41 GB.

B. Throughput Model

To evaluate the impact of fine-tuned SLMs on pacing gain decisions in BBR congestion control flows, we construct a surrogate approach that estimates the resulting throughput and retransmissions without requiring full TCP-in-the-loop replays. The surrogate model relies on the measured `iperf3` statistics from the BBR flows, and SLM/LLM-generated discrete pacing-gain actions. This approach enables scalable, model-agnostic evaluation of control policies.

$$b_{\text{send}}(i) = G(a_i) \widehat{B}_w(i), \quad (21)$$

A simplified version of the BBR sending rate can be given as the above equation, where $\widehat{B}_w(i)$ is the estimated bottleneck bandwidth, approximated by a 95-th percentile rolling window value $B_{\text{cap}}(i)$. Thus, the delivered throughput through SLM predicted pacing gains can be given as:

$$T^{\text{SLM}}(i) = B_{\text{cap}}(i) \cdot \min(G(a_i), 1.0). \quad (22)$$

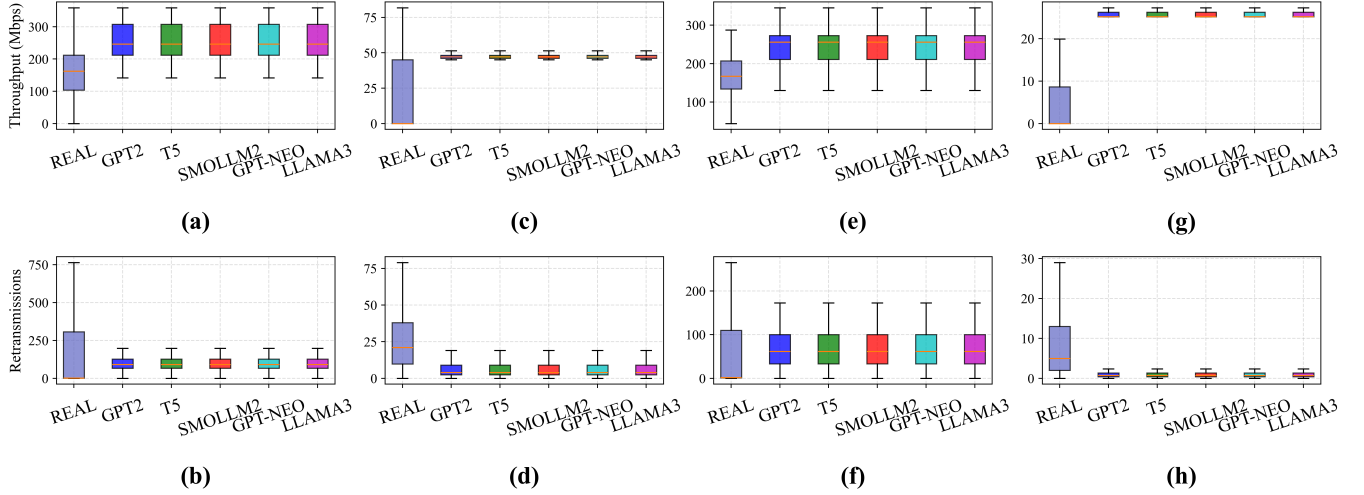


Fig. 9: Evaluation of SLM-predicted BBR pacing gains in terms of throughput and retransmissions, compared against native Tokyo BBR flows and the LLaMA 3.2 predictions. (a) Downlink individual flow throughput. (b) Downlink individual flow retransmissions. (c) Uplink individual flow throughput. (d) Uplink individual flow retransmissions. (e) Downlink competing flow throughput. (f) Downlink competing flow retransmissions. (g) Uplink competing flow throughput. (h) Uplink competing flow retransmissions.

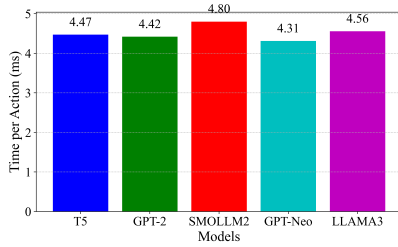


Fig. 10: Action generation time comparison in inference.

In Eq. (22), since probe-up or cruise resulted in $G(a_i) \geq 1$, throughput saturates at the bottleneck, and throughput is proportionally reduced in probe-down ($G(a_i) < 1$). When $G(a_i) > 1$, the sender transmits at a rate higher than the bottleneck capacity, even though this increases the amount of data in flight, the delivered throughput remains constrained by the bottleneck bandwidth. Consequently, the excess traffic accumulates in the bottleneck queue, leading to increased queuing delay and a higher probability of packet loss and retransmissions. Therefore, gains greater than one primarily manifest as elevated RTT and retransmissions rather than proportional throughput improvements.

C. Retransmission Model

To evaluate the impact of the fine-tuned language model predicted pacing gains on retransmission, we introduce a phase-aware methodology that maps the predicted pacing gain to an expected retransmission level. To model this effect smoothly, we define a shifted softplus activation approach ($\text{softplus}(x) = \ln(1 + e^x)$). The probe strength can be computed as:

$$S(G_i) = \max(\text{softplus}(\beta(G_i - 1)) - \text{softplus}(0), 0), \quad (23)$$

which guarantees $S(G_i) = 0$ when $G_i = 1$, ensuring no artificial penalty in cruise mode. The normalized probe-up

component is defined as:

$$\Phi(G_i) = \left(\frac{S(G_i)}{S(G_{\max})} \right)^\alpha \quad (24)$$

where G_{\max} is the maximum allowed pacing gain, parameters $\alpha = 1.5$ controls superlinear growth, and $\beta = 5$ controls sharpness. In the absence of probing, non-zero retransmissions occur due to wireless impairments and background contentions. This is represented through a small baseline term ϵ , ($\epsilon \ll 1$), where it sets the minimum loss floor.

Therefore, the instantaneous loss factor can be defined as:

$$L_i = U_i [\epsilon + (1 - \epsilon)\Phi(G_i)]. \quad (25)$$

ensuring retransmissions increase only when both utilization and probe aggressiveness are high.

For pacing gains below unity ($G_i < 1$), BBR intentionally drains queues. This effect is explicitly rewarded by reducing the loss factor:

$$L_i \leftarrow L_i (1 - \kappa_{\text{down}}(1 - G_i)), \quad (26)$$

where $\kappa_{\text{down}} \in (0, 1)$ controls the strength of the probe-down benefit. However, the final loss factor is limited to a valid range as $L_i = \min(\max(L_i, 0), 1)$. Therefore, the estimated retransmissions are obtained by scaling within the local congestion envelope:

$$\tau_i^{\text{SLM}} = \tau_{\min} + (\tau_{\max, i} - \tau_{\min}) L_i \quad (27)$$

where $\tau_{\max, i}$ is the rolling maximum of retransmissions, capturing the local congestion regime.

As discussed in § II, we captured BBR `iperf3` data for independent downlink, uplink streams, and parallel competitive downlink and uplink streams, which compete against another three CCAs: Hybla, Cubic, and Vegas across six cities. We leveraged Ohio, São Paulo, London, Mumbai, and Sydney BBR data to finetune the SLMs and LLaMA 3.2 LLM, and evaluate them with the Tokyo data set. SLM predicted BBR

spacing gain driven results for Tokyo are then compared against the actual data and LLaMA 3.2 model. Calculated throughput and retransmissions through the surrogate models discussed above are depicted in Fig. 9. Throughput and retransmission comparisons of the downlink and uplink for independent BBR streams are given in Fig. 9(a), Fig. 9(b), Fig. 9(c), and Fig. 9(d), respectively. Fig. 9(e), Fig. 9(f), Fig. 9(g), and Fig. 9(h) present the throughput and retransmission comparisons of competing downlink and uplink BBR streams. As shown in Fig. 10, we observe that the proposed LoRA approach reduces language model inference latency below 5 ms, which requires further extensive evaluation.

V. CONCLUSION

We present a framework to adapt SLM to improve BBR CCA for LEO satellite Internet. Through a globally distributed testbed over SpaceX's Starlink, we present an empirical evaluation of BBR characteristics in LEO satellite networks, highlighting its throughput advantage over other CCAs despite elevated retransmission rates. As a solution to the highlighted drawback, this work presents a SLM driven smooth pacing gain approach, reducing the inherent aggressiveness in BBR. Using four SLMs, we develop reward-maximizing expert action, evaluate the proposed approach and benchmark the results with a fine-tuned LLM and real BBR flows. Results evaluated via surrogate models reveal that the distilled SLMs retain throughput while reducing the retransmissions through intelligent pacing gain selection. Due to the lightweight deployment advantages offered by SLMs, our developed model represents a further step toward intelligence-driven network control over satellite Internet.

REFERENCES

- [1] S. Dou, Z. Guo, and K. L. Yeung, "Unleashing the potential of leo constellations in building resilient and low-latency control plane for swans," *IEEE Transactions on Networking*, 2025.
- [2] N. Cardwell, I. Swett, and J. Beshay, "BBR Congestion Control," IETF Congestion Control Working Group (CCWG), Internet-Draft draft-ietf-ccwg-bbr-03, Oct 2024. [Online]. Available: <https://datatracker.ietf.org/doc/html/draft-ietf-ccwg-bbr-03>
- [3] F. Wang *et al.*, "A Comprehensive Survey of Small Language Models in the Era of Large Language Models: Techniques, Enhancements, Applications, Collaboration with LLMs, and Trustworthiness," *ACM Transactions on Intelligent Systems and Technology*, vol. 16, no. 6, pp. 1–87, 2025.
- [4] C. V. Nguyen *et al.*, "A Survey on Small Language Models," in *Proceedings of the 15th RANLP*, Sep. 2025, pp. 807–821.
- [5] Z. Lin *et al.*, "Pushing large language models to the 6g edge: Vision, challenges, and opportunities," *IEEE Communications Magazine*, vol. 63, no. 9, pp. 52–59, 2025.
- [6] R. De Silva and S. R. Pokhrel, "Understanding bbr-v3 dynamics over starlink: An experimental evaluation of satellite internet," in *2026 40th International Conference on Information Networking (ICOIN)*. IEEE, 2026, pp. 119–122.
- [7] I. F. Akyildiz, G. Morabito, and S. Palazzo, "Tcp-peach: a new congestion control scheme for satellite ip networks," *IEEE/ACM Transactions on networking*, vol. 9, no. 3, pp. 307–321, 2002.
- [8] T. Taleb, N. Kato, and Y. Nemoto, "Refwa: An efficient and fair congestion control scheme for leo satellite networks," *IEEE/ACM transactions on networking*, vol. 14, no. 5, pp. 1031–1044, 2006.
- [9] J. Garcia, S. Sundberg, and A. Brunstrom, "Tcp congestion control performance over starlink," ser. ANRW '25. New York, NY, USA: Association for Computing Machinery, 2025, p. 70–77. [Online]. Available: <https://doi.org/10.1145/3744200.3744760>
- [10] Z. Lai *et al.*, "LeoCC: Making Internet Congestion Control Robust to LEO Satellite Dynamics," in *Proceedings of the ACM SIGCOMM 2025 Conference*, 2025, pp. 129–146.
- [11] V. Kamel, J. Zhao, D. Li, and J. Pan, "Starquic: Tuning congestion control algorithms for quic over leo satellite networks," in *Proceedings of the 2nd International Workshop on LEO Networking and Communication*, 2024, pp. 43–48.
- [12] Y. Zhang, L. Cui, and F. P. Tso, "Modest bbr: Enabling better fairness for bbr congestion control," in *2018 IEEE symposium on computers and communications (ISCC)*. IEEE, 2018, pp. 00646–00651.
- [13] Y.-J. Song, G.-H. Kim, and Y.-Z. Cho, "Bbr-cws: Improving the inter-protocol fairness of bbr," *Electronics*, vol. 9, no. 5, p. 862, 2020.
- [14] I. Mahmud, G.-H. Kim, T. Lubna, and Y.-Z. Cho, "Bbr-acd: Bbr with advanced congestion detection," *Electronics*, vol. 9, no. 1, p. 136, 2020.
- [15] S. Zheng, J. Liu, X. Yan, Z. Xing, X. Di, and H. Qi, "Bbr-r: Improving bbr performance in multi-flow competition scenarios," *Computer Networks*, vol. 254, p. 110816, 2024.
- [16] C. K. Njogu, W. Yang, H. W. Njogu, and A. Bosire, "Bbr-with enhanced fairness (bbr-efra): A new enhanced rtt fairness for bbr congestion control algorithm," *Computer communications*, vol. 200, pp. 95–103, 2023.
- [17] Z. Han and G. Hasegawa, "Bbr-es: an extended-state optimization for bbr congestion control," *IEEE Transactions on Network and Service Management*, 2026.
- [18] P. K. Donta, S. N. Srirama, T. Amgoth, and C. S. R. Annavarapu, "icocoa: Intelligent congestion control algorithm for coap using deep reinforcement learning," *Journal of Ambient Intelligence and Humanized Computing*, vol. 14, no. 3, pp. 2951–2966, 2023.
- [19] Y. Zhu, "Intelligent Congestion Control of Data Transmission in Low Earth Orbit Satellite Networks Based on Reinforcement Learning: Analysis and Optimization," *Information Sciences*, vol. 694, p. 121692, 2025.
- [20] Y. Yan *et al.*, "A handover-aware congestion control algorithm assisted by drl in leo satellite networks," in *ICC*. IEEE, 2025, pp. 4720–4725.
- [21] Z. Xing, H. Qi, X. Di, J. Liu, and L. Cong, "Deep reinforcement learning based congestion control mechanism for sdn and ndn in satellite networks," in *International Conference on Mobile Wireless Middleware, Operating Systems, and Applications*. Springer, 2022, pp. 13–29.
- [22] A. Masood *et al.*, "Intelligent tcp congestion control scheme in internet of deep space things communication," *IEEE Transactions on Network Science and Engineering*, vol. 10, no. 3, pp. 1472–1486, 2022.
- [23] S. R. Pokhrel, D. Satish, J. Kua, and A. Walid, "Distilling large language models for network active queue management," *IEEE Transactions on Networking*, 2026.
- [24] D. Wu, X. Wang, Y. Qiao, Z. Wang, J. Jiang, S. Cui, and F. Wang, "NetLLM: Adapting Large Language Models for Networking," in *Proceedings of the ACM SIGCOMM 2024 Conference*, ser. ACM SIGCOMM '24. New York, NY, USA: Association for Computing Machinery, 2024, p. 661–678. [Online]. Available: <https://doi.org/10.1145/3651890.3672268>
- [25] R. De Silva and S. Raj Pokhrel, "Adapting Large Language Models for Cognitive Spectrum Allocation in Coexisting GEO-LEO Satellites," in *2025 IEEE 50th Conference on Local Computer Networks (LCN)*, 2025, pp. 1–6.
- [26] H. Chen *et al.*, "Towards edge general intelligence via large language models: Opportunities and challenges," *IEEE Network*, 2025.
- [27] S. Ha, I. Rhee, and L. Xu, "Cubic: a new tcp-friendly high-speed tcp variant," *ACM SIGOPS operating systems review*, vol. 42, no. 5, pp. 64–74, 2008.
- [28] L. S. Brakmo and L. L. Peterson, "TCP Vegas: End to End Congestion Avoidance on a Global Internet," *IEEE Journal on Selected Areas in Communications*, vol. 13, no. 8, pp. 1465–1480, 2002.
- [29] C. Caini and R. Firrincieli, "Tcp hybla: a tcp enhancement for heterogeneous networks," *International journal of satellite communications and networking*, vol. 22, no. 5, pp. 547–566, 2004.
- [30] F. Yang, Q. Wu, Z. Li, Y. Liu, G. Pau, and G. Xie, "Bbrv2+: Towards balancing aggressiveness and fairness with delay-based bandwidth probing," *Computer Networks*, vol. 206, p. 108789, 2022.
- [31] Z. Wang *et al.*, "An Improved BBR Algorithm with Adaptive Congestion Control for LEO Satellite Networks," in *2024 International Conference on Cloud and Network Computing (ICNC)*. IEEE, 2024, pp. 23–29.
- [32] L. Xu *et al.*, "Parameter-efficient Fine-tuning Methods for Pretrained Language Models: A Critical Review and Assessment," *Nature Machine Intelligence*, 2023.
- [33] L. Huang *et al.*, "A survey on hallucination in large language models: Principles, taxonomy, challenges, and open questions," *ACM Transactions on Information Systems*, vol. 43, no. 2, pp. 1–55, 2025.